Acceleration of on-axis and ring-shaped electron beams in wakefields driven by Laguerre-Gaussian pulses

Guo-Bo Zhang,[1,2] Min Chen,[2,3,a)] Ji Luo,[2,3] Ming Zeng,[2,3] Tao Yuan,[2,3] Ji-Ye Yu,[2,3] Yan-Yun Ma,[1,3,a)] Tong-Pu Yu,[1] Lu-Le Yu,[2,3] Su-Ming Weng,[2,3] and Zheng-Ming Sheng[2,3,4]
[1]*College of Science, National University of Defense Technology, Changsha 410073, China*
[2]*Key Laboratory for Laser Plasmas (MOE) and Department of Physics and Astronomy, Shanghai Jiao Tong University, Shanghai 200240, China*
[3]*Collaborative Innovation Center of IFSA (CICIFSA), Shanghai Jiao Tong University, Shanghai 200240, China*
[4]*SUPA, Department of Physics, University of Strathclyde, Glasgow G4 0NG, United Kingdom*

(Received 3 January 2016; accepted 25 February 2016; published online 9 March 2016)

The acceleration of electron beams with multiple transverse structures in wakefields driven by Laguerre-Gaussian pulses has been studied through three-dimensional (3D) particle-in-cell simulations. Under different laser-plasma conditions, the wakefield shows different transverse structures. In general cases, the wakefield shows a donut-like structure and it accelerates the ring-shaped hollow electron beam. When a lower plasma density or a smaller laser spot size is used, besides the donut-like wakefield, a central bell-like wakefield can also be excited. The wake sets in the center of the donut-like wake. In this case, both a central on-axis electron beam and a ring-shaped electron beam are simultaneously accelerated. Further, reducing the plasma density or laser spot size leads to an on-axis electron beam acceleration only. The research is beneficial for some potential applications requiring special pulse beam structures, such as positron acceleration and collimation. © *2016 AIP Publishing LLC*. [http://dx.doi.org/10.1063/1.4943419]

I. INTRODUCTION

Laser wakefield acceleration (LWFA) has shown great potential to be the candidate for the next generation of table-top electron accelerator and radiation source because of its tremendous acceleration gradient which usually can be as large as one thousand times of a traditional RF accelerator.[1–3] An intense plasma wake can be excited by an ultra-short (with duration $c\tau < \lambda_p$, where λ_p is the wavelength of the plasma wave and c is the speed of light in vacuum) and ultra-intense (with normalized laser intensity $a = eE/m_e\omega_0 c \geq 1$) laser pulse propagating in an underdense plasma. The ponderomotive force of the driver pulse expels out the background electrons and leaves a cavity made of immobile ions following the laser pulse. Some trapped electrons can be accelerated by the large acceleration field (about $E(\mathrm{V/m}) \approx 96\sqrt{n_0(\mathrm{cm}^{-3})}$) inside the moving cavity, where n_0 denotes the background plasma density.[4] Nowadays, most of the theoretical and experimental studies on LWFA make use of the Gaussian shaped laser pulses both in transverse and longitudinal directions. In such cases, a linear sine-shape or a nonlinear spherical bubble-like wake structure is generated and electrons are usually only accelerated around the axis and the whole beam shows a linear structure. Studies focusing on the beam quality improvement by controlling the injection process have been extensively investigated.[5–10] Recently, electron beams with extremely low energy spread and emittance are demonstrated,[11–15] which can be used for the applications such as x-ray generation,[16,17] positron pulse production,[18] and attosecond electron.[19] However, for certain applications, the beam shape itself is also an important factor. Beams with controllable transverse modes may have much wider applications such as hollow electron beam for positron beam collimation and acceleration.[20] Nevertheless, due to the extremely small size of the plasma wake, shaping an electron beam during acceleration is difficult unless the plasma wake itself has special structures. In recent years, wake shaping by using combined driver laser pulses or laser pulse with relatively large focus size were studied.[21,22] Besides this scheme, using single driver pulse with a special transverse mode is an alternative way for special plasma wake generation such as using Laguerre-Gaussian (LG) pulse.[23,24] Theoretical studies have shown that intense LG pulses can be obtained by reflecting intense normal Gaussian pulses from a plasma plate with helical thickness.[25] This kind of driver pulse has already been proposed to generate x-rays with orbit angular momentum (OAM)[26] and intense high-order optical vortices.[27] In our previous studies, we also found that by using ionization injection, a ring-shaped electron beam can rotate transversely during the acceleration by the donut-like plasma wake driven by LG pulse.[24]

In this paper, we revisited this problem by investigating a wider regime of laser plasma conditions and found that electron beams with multiple transverse structures can be generated. Full 3D-particle-in-cell (PIC) simulations show that besides the normal donut-like wake, a closed bell-like wake sets in the center of the donut-like wake and it can accelerate a central on-axis electron beam under suitable laser-plasma conditions. Moreover, the transition from a ring-shaped electron beam to simultaneous on-axis and ring-shaped beams is controllable by tuning the plasma density and laser spot size.

[a)]Authors to whom correspondence should be addressed. Electronic addresses: minchen@sjtu.edu.cn and yanyunma@126.com

II. MULTIPLE TRANSVERSE WAKEFIELDS GENERATION AND ELECTRON BEAMS ACCELERATION

To see the transverse wake structure evolution, we performed a series of 3D-PIC simulations by using the code OSIRIS.[23,28] We first fixed the laser parameters and varied the background plasma density only. The simulation box size is $50\mu m \times 50\mu m \times 40\mu m$, which is sampled by $300 \times 300 \times 600$ cells. A Laguerre-Gaussian laser pulse with linear polarization along the x-direction and propagates along the z-direction with LG mode (1, 0) is given by $a(r,\xi) = a_0 r w_0^{-1} \exp(-r^2/w_0^2 - \xi^2/(c\tau)^2 + i\theta)$. Where $a_0 = eE_0/m_e\omega_0 c = 3.2$ is the normalized peak intensity of the laser electric field, E_0 is the laser electric field, and $\omega_0 = 2\pi c/\lambda_0$ is the laser frequency with wavelength of $\lambda_0 = 0.8\mu m$, m_e and e are the electron rest mass and charge, respectively. The laser spot radius is $w_0 = 10\mu m$, and the pulse duration is $\tau = 13.2$ fs. $r = \sqrt{x^2 + y^2}$ is the radial distance to the axis, x and y are the transverse coordinates, $\xi = z - ct$ is the forward co-moving coordinate with the laser, θ is the azimuthal angle. In the simulations, we utilized a moving window and took fully ionized hydrogen plasma with a trapezoidal density profile: 15 μm linear up-ramp, 300 μm plateau, and 15 μm linear down-ramp. In order to illustrate the transition from a ring-shaped electron beam to a central on-axis electron beam, three typical plasma densities were used. Case 1: $n_e = 1.98 \times 10^{19}\text{cm}^{-3}$, $k_p w_0 = 8.5$; case 2: $n_e = 1.13 \times 10^{19}\text{cm}^{-3}$, $k_p w_0 = 6.4$; and case 3: $n_e = 0.28 \times 10^{19}\text{cm}^{-3}$, $k_p w_0 = 3.2$. These parameters cover the regimes of both rough separation and overlapping condition (i.e., $k_p w_0 = 2\sqrt{2a_0}$) for the inner electron sheaths of a normal donut-like wake.[23]

Figure 1 shows the central slice images of the wake at two different instants of these three simulations. Typical trajectories of background electrons are also shown by the green lines in Figs. 1(a)–1(c). The z-axis of the trajectories is $Z_e - ct$, which means the trajectories represent the one in the

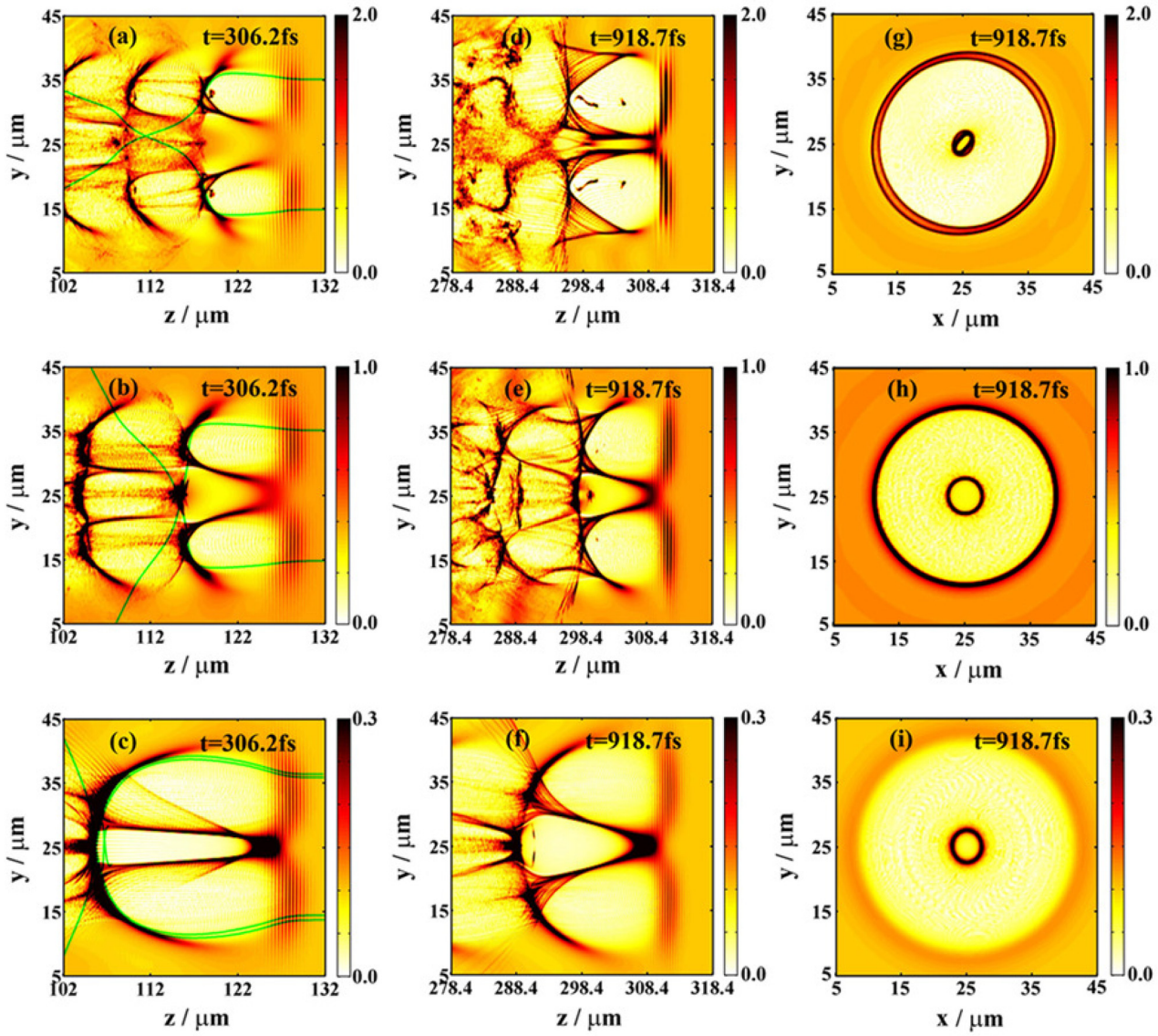

FIG. 1. Transverse slice images of electron density distribution of case 1 [(a) and (d)], case 2 [(b) and (e)], case 3 [(c) and (f)] at t = 306.2 fs and t = 918.7 fs, respectively. Longitudinal slice images of electron density distribution of case 1 (g), case 2 (h), and case 3 (i) at z = 303.4 μm. The green lines in (a)–(c) represent typical background electron trajectories in the wake rest frame. The normalized electron density unit is 2.829×10^{19} cm^{-3}.

wake rest frame. As one can see clearly from Fig. 1(a) that, when the plasma density is high (in case 1), there are two separate bubbles in the slice image. In the three dimensional geometry, this corresponds to an annular single donut-like wake. The front of the two bubble structures are not overlapped due to the relatively large laser spot size and the small plasma wavelength. Typical electrons trajectories in Fig. 1(a) also show the back of the bubble is completely separated. In this case, only a donut-like bubble can be formed. Along with the laser pulse experiencing self-focusing, the bubble size increases and electrons are self-injected into the wake forming a ring-shaped electron beam as shown in Figs. 1(d) and 1(g). When the plasma density gets lower, the bubble size increases (bubble radius $r_b \propto n_e^{-1/2}$). The front parts of the inner electron sheaths of the ring-shaped wake begin to be overlapped. And the background electrons can get much stronger transverse acceleration which makes the trajectories cross point moving close to the end of the donut-like bubble as shown by the green trajectories in Fig. 1(b). A bell-like central wake begins to form. The transverse slice image appears multiple transverse wakefield structures. The central bell-like wake can also accelerate an on-axis electron beam. Finally, the simulation shows a central linear electron beam and an outer ring-shaped electron beam are simultaneously accelerated as shown in Figs. 1(e) and 1(h). When the density is further decreased, electrons are transversely piled up on axis by the ponderomotive force of the LG pulse. The electrons also cross each other at the end of the bubble and form a closed central bubble structure as shown in Fig. 1(c). The multiple transverse wakefields become more clearly. In this case, the outer ring-shaped electron beam disappears because the electrons are much easier to be injected into the central bubble (see the green trajectory in Fig. 1(c)) than the donut-like bubble. Only a central on-axis electron beam is formed and accelerated (shown in Figs. 1(f) and 1(i)).

To show the central wake acceleration ability, we presented the transverse slice images of the acceleration field E_z and focusing field $E_y - B_x$ in Figs. 2 and 3. Comparing Figs. 2(a)–2(c), one can see different accelerating fields for these three cases. A clearly donut-like accelerating field can be seen in Fig. 2(a). The central acceleration field is very weak. Figures 2(b) and 2(c) show that the central accelerating field becomes much clearer and stronger. Especially in Fig. 2(c), the acceleration fields of the donut-like wake and the central wake have similar intensities. They merge with each other. Figure 2(d) shows the corresponding on-axis accelerating fields. Although the intensity of donut-like acceleration field is decreasing, i.e., $\propto n_e^{1/2}$, the central on-axis acceleration field is gradually increased. In the simulations, we found that the maximum central acceleration field in the first bubble can reach 338 GV/m for case 3. It deserves to point out that, in all of these cases, the central wakes can be formed far behind the driver pulse. However, these structures show chaos characters, which are unstable and difficult for stable acceleration.

The spatial distributions of the focusing fields in the plane of x = 25 μm are shown in Figs. 3(a)–3(c). As one can see along with the formation of the central wake, the central focusing fields are also generated. Different from a normal bubble structure, the focusing fields in the central region show an inverted triangle-like shape, and the intensity of the fields is relatively weaker than the outer wakefields as shown in Fig. 3(d). The transverse gradient of the fields is also very small, which is similar as the one in a hollow channel wakefield.[29]

Energy spectra of the trapped electrons corresponding to the above three cases are shown in Fig. 4. One can see that a

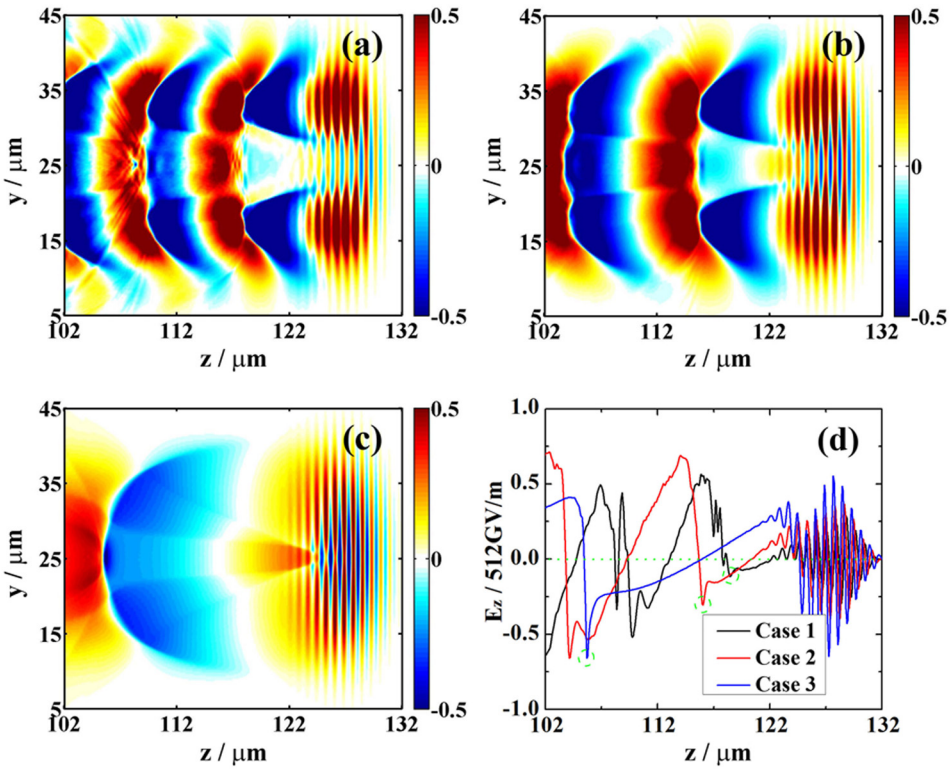

FIG. 2. Transverse slice images of the longitudinal accelerating fields E_z of case 1 (a), case 2 (b), and case 3 (c) at t = 306.2 fs. (d) The corresponding on-axis fields at $y = 25\mu$m. The normalized field unit is 512 GV/m.

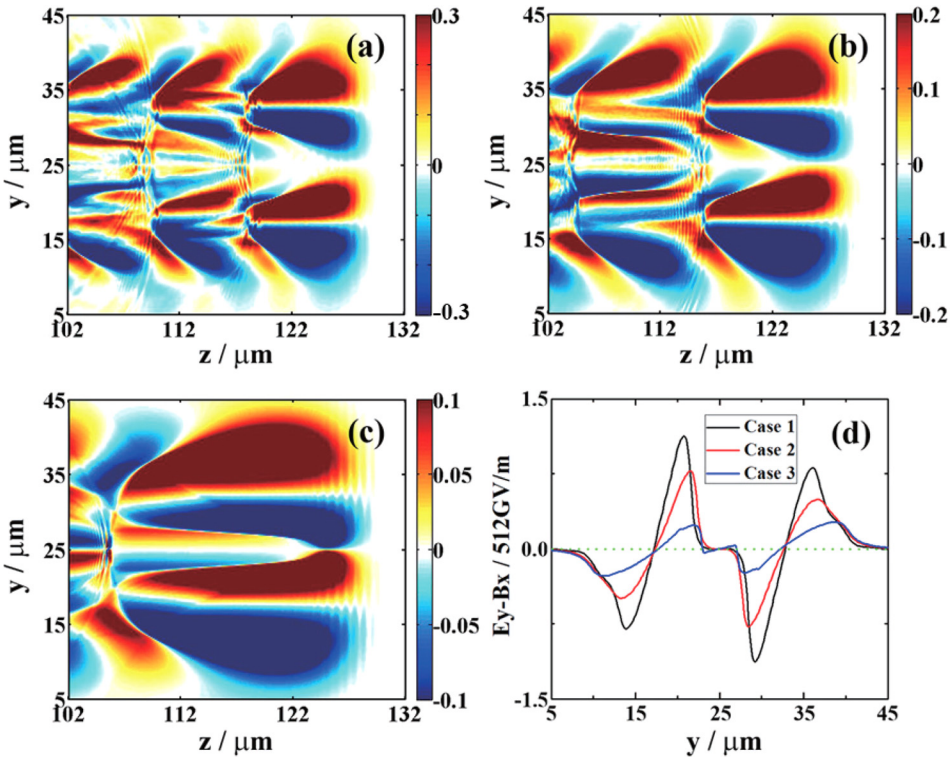

FIG. 3. Spatial distribution of transverse focusing fields $E_y - B_x$ in the plane of $x = 25\mu$m of case 1 (a), case 2 (b), case 3 (c) at t = 306.2 fs. (d) The corresponding profiles of the focusing fields at each bubble center. The normalized field unit is 512 GV/m.

continuous spectrum of the ring-shaped electron beam (blue line) in case 1 is formed due to the poor control of the electron injection process. In case 2 (red line), there are two peaks with energies of 102 MeV and 29 MeV, respectively. The high energy peak corresponds to the ring-shaped electron beam and the low energy peak corresponds to the central on-axis electron beam. It is because that the central acceleration field is much smaller than the donut-like wakefield. For the lower density case (black line), the trapped central electron beam shows a quasi-monoenergetic peak of 34 MeV, which is similar as the second energy peak in case 2.

III. TRANSITION FROM A RING-SHAPED ELECTRON BEAM TO A CENTRAL ON-AXIS ELECTRON BEAM

To investigate the relationship between the laser-plasma parameters and the transition of the wake structures, we made parameter scans by changing the plasma density and the laser spot size. The evolution of the trapped electron charge with the two parameters is shown in Fig. 5. We analyzed the electron acceleration process and used the shaded colors to divide the parameters for electron acceleration with different transverse structures. The orange shaded region marks the area with only a central on-axis electron beam acceleration, the green shaded region marks the area with two kinds of electron beams acceleration, and the yellow ones mark only a ring-shaped electron beam acceleration. Three sets of typical trapped electron trajectories are also shown in Figs. 5(b)–5(d). The colors along the trajectories represent the longitudinal momentum. One can clearly see that the central electron beam originally come from the outer electron sheaths of the donut-like bubble. The electrons can only be injected into the central bubble at lower plasma density due to the lower injection threshold there and the easier transverse cross from the donut-like bubble to the central bubble as shown in Fig. 5(b). When the plasma density gradually increases, the electrons can be injected into both the central bell-like and outer donut-like bubbles. The trapped electron beam transforms from central linear shape to the combined on-axis and ring-shaped beams. Figure 5(d) shows the trapped electron trajectories with the higher plasma density case, where only a ring-shaped beam is formed. The trapped electrons come from the sheaths of the donut-like bubble.

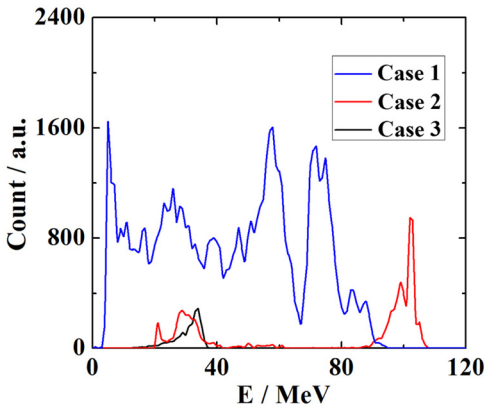

FIG. 4. Energy spectra of trapped electrons for these three cases at t = 1148.4 fs.

According to the previous studies, one can see that the generation of multiple transverse wakefields is because of the inner electron sheaths of the donut-like wake overlapping in the front part and closing at the end. Therefore, varying the plasma density is not the only way to form the central bell-like bubble. One can also realize it by adjusting the laser spot size. The trapped electron charge evolution with the laser spot size at t = 1148.4 fs by fixing the plasma density

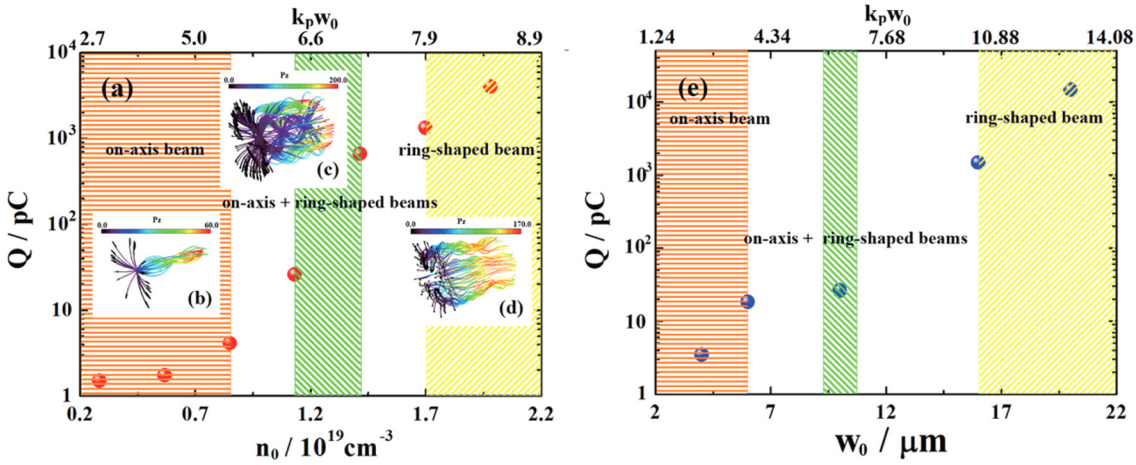

FIG. 5. (a) 3D-PIC simulation results of the trapped electron charge as a function of the plasma density at t = 1148.4 fs. The orange shaded region marks the parameters with which only on-axis electron beam acceleration occurs. The green shaded region corresponds to two beams acceleration. The yellow shaded region corresponds to the only ring-shaped electron beam acceleration. (b)–(d) Represent the trajectories of the trapped electrons. (e) The trapped electron charge evolution with various laser spot sizes at t = 1148.4 fs. The plasma density is fixed to be $n_e = 1.13 \times 10^{19}\text{cm}^{-3}$. The shaded regions mark the transition process of multiple transverse wakefields from a central on-axis electron beam to a ring-shaped electron beam.

$n_e = 1.13 \times 10^{19}\text{cm}^{-3}$ is shown in Fig. 5(e). The maximum trapped ring-shaped electron beam charge can be up to 14.8 nC with the LG laser spot radius of $k_p w_0 = 12.8$. The shaded regions mark the evolution process similar to that in Fig. 5(a). One can see the same transform process like adjusting the plasma density. For the small spot size, there is a clearly bell-like central bubble structure due to the closing distance of inner electron sheaths of donut-like bubble. Likewise, a larger distance of the inner electron sheaths cannot form the central bell-like structure. The electron acceleration process is also similar to the studies before.

IV. SUMMARY

In summary, we have studied the generation and transition of multiple transverse wakefields by using Laguerre-Gaussian pulse. 3D PIC simulations show that a donut-like wake is usually formed, and it can accelerate ring-shaped self-injected hollow electron beam. However, under suitable conditions (lower plasma density or small laser spot size), the inner electron sheaths of the donut-like wake will overlap in the front part of the wake, and the sheath electrons pile up on-axis. The trajectories of the background electrons cross each other near the end of the donut-like bubble forming a closed central bell-like wake. The wake has a longitudinal acceleration field and an inverted triangle-like transverse focusing field. The multiple transverse wakefields can accelerate both on-axis and ring-shaped electron beams simultaneously. One can control the transition process from a central on-axis electron beam to a ring-shaped electron beam by tuning the plasma and laser parameters. These special electron beam structures may have potential applications where multi or special structure beams are required. For example, the simultaneous on-axis and ring-shaped beams, the ring-shaped beam can accelerate the on-axis beam through dielectric wakefield accelerator.[30] And the ring-shaped electron beam can be used for x-ray radiation with hollow center distribution and wakefield excitation suit for proton acceleration.

ACKNOWLEDGMENTS

This work was supported by the National Basic Research Program of China (Grant No. 2013CBA01504), the National Science Foundation of China (Grant Nos. 11374209, 11374210, 11475260, 11405107, 11474360, and 11375265). M.C. appreciates the support from national 1000 Youth Talent Project of China. The authors would like to acknowledge the OSIRIS Consortium, consisting of UCLA and IST (Lisbon, Portugal) for the use of OSIRIS and the visXD framework. Simulations were performed on the Π supercomputer at Shanghai Jiao Tong University and Tianhe II supercomputer at Guangzhou.

[1]T. Tajima and J. M. Dawson, Phys. Rev. Lett. **43**, 267 (1979).
[2]E. Esarey, C. B. Schroeder, and W. P. Leemans, Rev. Mod. Phys. **81**, 1229 (2009).
[3]S. Corde, K. Ta Phuoc, G. Lambert, R. Fitour, V. Malka, A. Rousse, A. Beck, and E. Lefebvr, Rev. Mod. Phys. **85**, 1 (2013); M. Chen, J. Luo, F. Y. Li, F. Liu, Z. M. Sheng, and J. Zhang, Light: Sci. Appl. **5**, e16015 (2016).
[4]A. Pukhov and J. Meyer-ter-vehn, Appl. Phys. B **74**, 355–361 (2002).
[5]M. Z. Mo, A. Ali, S. Fourmaux, P. Lassonde, J. C. Kieffer, and R. Fedosejevs, Appl. Phys. Lett. **102**, 134102 (2013).
[6]M. Chen, Z. M. Sheng, Y. Y. Ma, and J. Zhang, J. Appl. Phys. **99**, 056109 (2006); M. Chen, E. Esarey, C. B. Schroeder, C. G. R. Geddes, and W. P. Leemans, Phys. Plasmas **19**, 033101 (2012).
[7]A. J. Gonsalves, K. Nakamura, C. Lin, D. Panasenko, S. Shiraishi, T. Sokollik, C. Benedetti, C. B. Schroeder, C. G. R. Geddes, J. van Tilborg, J. Osterhoff, E. Esarey, C. Toth, and W. P. Leemans, Nat. Phys. **7**, 862–866 (2011).
[8]Y. Y. Ma, S. Kawata, T. P. Yu, Y. Q. Gu, Z. M. Sheng, M. Y. Yu, H. B. Zhuo, H. J. Liu, Y. Yin, K. Takahashi, X. Y. Xie, J. X. Liu, C. L. Tian, and F. Q. Shao, Phys. Rev. E **85**, 046403 (2012).
[9]W. P. Leemans, A. J. Gonsalves, H. S. Mao, K. Nakamura, C. Benedetti, C. B. Schroeder, Cs. Tóth, J. Daniels, D. E. Mittelberger, S. S. Bulanov, J. L. Vay, C. G. R. Geddes, and E. Esarey, Phys. Rev. Lett. **113**, 245002 (2014).
[10]X. Davoine, E. Lefebvre, C. Rechatin, J. Faure, and V. Malka, Phys. Rev. Lett. **102**, 065001 (2009).
[11]A. J. Goers, S. J. Yoon, J. A. Elle, G. A. Hine, and H. M. Milchberg, Appl. Phys. Lett. **104**, 214105 (2014).

[12]L. L. Yu, E. Esarey, C. B. Schroeder, J. L. Vay, C. Benedetti, C. G. R. Geddes, M. Chen, and W. P. Leemans, Phys. Rev. Lett. **112**, 125001 (2014).
[13]B. B. Pollock, C. E. Clayton, J. E. Ralph, F. Albert, A. Davidson, L. Divol, C. Filip, S. H. Glenzer, K. Herpoldt, W. Lu, K. A. Marsh, J. Meinecke, W. B. Mori, A. Pak, T. C. Rensink, J. S. Ross, J. Shaw, G. R. Tynan, C. Joshi, and D. H. Froula, Phys. Rev. Lett. **107**, 045001 (2011).
[14]M. Zeng, M. Chen, L. L. Yu, W. B. Mori, Z. M. Sheng, B. Hidding, D. A. Jaroszynski, and J. Zhang, Phys. Rev. Lett. **114**, 084801 (2015).
[15]O. Lundh, J. Lim, C. Rechatin, L. Ammoura, A. Ben-Ismaïl, X. Davoine, G. Gallot, J. P. Goddet, E. Lefebvre, V. Malka, and J. Faure, Nat. Phys. **7**, 219 (2011).
[16]F. V. Hartemann, D. J. Gibson, W. J. Brown, A. Rousse, K. Ta Phuoc, V. Malka, J. Faure, and A. Pukhov, Phys. Rev. Spec. Top. Accel. Beams **10**, 011301 (2007).
[17]J. M. Cole, J. C. Wood, N. C. Lopes, K. Poder, R. L. Abel, S. Alatabi, J. S. J. Bryant, A. Jin, S. Kneip, K. Mecseki, D. R. Symes, S. P. D. Mangles, and Z. Najmudin, Sci. Rep. **5**, 13244 (2015); T. P. Yu, A. Pukhov, Z. M. Sheng, F. Liu, and G. Shvets, Phys. Rev. Lett. **110**, 045001 (2013).
[18]B. E. Blue, C. E. Clayton, C. L. O'Connell, F. J. Decker, M. J. Hogan, C. Huang, R. Iverson, C. Joshi, T. C. Katsouleas, W. Lu, K. A. Marsh, W. B. Mori, P. Muggli, R. Siemann, and D. Walz, Phys. Rev. Lett. **90**, 214801 (2003).
[19]H. C. Wu, J. Meyer-ter-Vehn, J. Fernández, and B. M. Hegelich, Phys. Rev. Lett. **104**, 234801 (2010).
[20]N. Jain, T. M. Antonsen, and J. P. Palastro, Phys. Rev. Lett. **115**, 195001 (2015).
[21]E. Cormier-Michel, E. Esarey, C. G. R. Geddes, C. B. Schroeder, K. Paul, P. J. Mullowney, J. R. Cary, and W. P. Leemans, Phys. Rev. Spec. Top. Accel. Beams **14**, 031303 (2011); L. L. Yu, C. B. Schroeder, F. Y. Li, C. Benedetti, M. Chen, S. M. Weng, Z. M. Sheng, and E. Esarey, Phys. Plasmas **21**, 120702 (2014).
[22]J. C. Xu, B. F. Shen, X. M. Zhang, M. Wen, L. L. Ji, W. P. Wang, Y. H. Yu, and K. Nakajima, New J. Phys. **12**, 023037 (2010).
[23]J. Vieira and J. T. Mendonça, Phys. Rev. Lett. **112**, 215001 (2014).
[24]G. B. Zhang, M. Chen, C. B. Schroeder, J. Luo, M. Zeng, F. Y. Li, L. L. Yu, S. M. Weng, Y. Y. Ma, T. P. Yu, Z. M. Sheng, and E. Esarey, "Acceleration and evolution of a hollow electron beam in wakefields driven by a Laguerre-Gaussian laser pulse," Phys. Plasmas. (submitted).
[25]Y. Shi, B. F. Shen, L. G. Zhang, X. M. Zhang, W. P. Wang, and Z. Z. Xu, Phys. Rev. Lett. **112**, 235001 (2014).
[26]L. Allen, M. Beijersbergen, R. Spreeuw, and J. Woerdman, Phys. Rev. A **45**, 8185–8189 (1992).
[27]X. M. Zhang, B. F. Shen, Y. Shi, X. F. Wang, L. G. Zhang, W. P. Wang, J. C. Xu, L. Q. Yi, and Z. Z. Xu, Phys. Rev. Lett. **114**, 173901 (2015).
[28]R. A. Fonseca, L. O. Silva, F. S. Tsung, V. K. Decyk, W. Lu, C. Ren, W. B. Mori, S. Deng, S. Lee, T. Katsouleas, and J. C. Adam, Lect. Notes Comput. Sci. **2331**, 342 (2002).
[29]A. Pukhov, O. Jansen, T. Tueckmantel, J. Thomas, and I. Yu. Kostyukov, Phys. Rev. Lett. **113**, 245003 (2014).
[30]G. V. Sotnikov, T. C. Marshall, and J. L. Hirshfield, Phys. Rev. Spec. Top. Accel. Beams **12**, 061302 (2009).